

SANDIA REPORT

SAND98-1407

Unlimited Release

Printed June 1998

Estimation of Constitutive Parameters for the Belridge Diatomite, South Belridge Diatomite Field

A. F. Fossum, J. T. Fredrich

Prepared by
Sandia National Laboratories
Albuquerque, New Mexico 87185 and Livermore, California 94550

Sandia is a multiprogram laboratory operated by Sandia Corporation,
a Lockheed Martin Company, for the United States Department of
Energy under Contract DE-AC04-94AL85000.

Approved for public release; further dissemination unlimited.



Sandia National Laboratories

Issued by Sandia National Laboratories, operated for the United States Department of Energy by Sandia Corporation.

NOTICE: This report was prepared as an account of work sponsored by an agency of the United States Government. Neither the United States Government nor any agency thereof, nor any of their employees, nor any of their contractors, subcontractors, or their employees, makes any warranty, express or implied, or assumes any legal liability or responsibility for the accuracy, completeness, or usefulness of any information, apparatus, product, or process disclosed, or represents that its use would not infringe privately owned rights. Reference herein to any specific commercial product, process, or service by trade name, trademark, manufacturer, or otherwise, does not necessarily constitute or imply its endorsement, recommendation, or favoring by the United States Government, any agency thereof, or any of their contractors or subcontractors. The views and opinions expressed herein do not necessarily state or reflect those of the United States Government, any agency thereof, or any of their contractors.

Printed in the United States of America. This report has been reproduced directly from the best available copy.

Available to DOE and DOE contractors from
Office of Scientific and Technical Information
P.O. Box 62
Oak Ridge, TN 37831

Prices available from (615) 576-8401, FTS 626-8401

Available to the public from
National Technical Information Service
U.S. Department of Commerce
5285 Port Royal Rd
Springfield, VA 22161

NTIS price codes
Printed copy: A03
Microfiche copy: A01



SAND98-1407
Unlimited Release
Printed June 1998

Estimation of Constitutive Parameters for the Belridge Diatomite, South Belridge Diatomite Field

A.F. Fossum

Engineering and Manufacturing Mechanics Department

J.T. Fredrich

Geomechanics Department

Sandia National Laboratories

P.O. Box 5800

Albuquerque, NM 87185-0751

Abstract

A cooperative national laboratory/industry research program was initiated in 1994 that improved understanding of the geomechanical processes causing well casing damage during oil production from weak, compactible formations. The program focused on the shallow diatomaceous oil reservoirs located in California's San Joaquin Valley, and combined analyses of historical field data, experimental determination of rock mechanical behavior, and geomechanical simulation of the reservoir and overburden response to production and injection. Sandia National Laboratories' quasi-static, large-deformation structural mechanics finite element code JAS3D was used to perform the three-dimensional geomechanical simulations. One of the material models implemented in JAS3D to simulate the time-independent inelastic (non-linear) deformation of geomaterials is a generalized version of the Sandler and Rubin cap plasticity model (Sandler and Rubin, 1979). This report documents the experimental rock mechanics data and material cap plasticity models that were derived to describe the Belridge Diatomite reservoir rock at the South Belridge Diatomite Field, Section 33.

This page intentionally left blank.

Acknowledgments

This work was performed as part of a Work For Others Agreement with Aera Energy LLC (previously CalResources LLC) under the direction of Tom Moroney (Aera Energy LLC) and Greg Deitrick (Shell E&P Tech. Co.). Publication of this report was supported by the U.S. Department of Energy's Natural Gas and Oil Technology Partnership Program (Fossil Energy).

This page intentionally left blank.

Table of Contents

Introduction	1
General Description of Belridge Diatomite Reservoir	3
Description of Sandia and ABAQUS Cap Models	3
Mathematical Description of the ESR Cap Model	4
Constitutive Models for Belridge Diatomite	7
Experimental Data Provided by Shell E&P Tech. Co.	7
Constitutive Parameter Estimation	7
Summary Remarks on Experimental Data	12
Constitutive Parameters and Comparative Plots.....	13
Conclusion	28
References	29

This page intentionally left blank.

Figures

Figure 1	Composite yield surface representation for the ESR Cap plasticity model	5
Figure 2	ESR Cap model versus ABAQUS cap model (J cycle data)	14
Figure 3	Measured versus predicted uniaxial strain response (J cycle runs)	15
Figure 4	Measured versus predicted uniaxial strain response (J cycle runs)	15
Figure 5	ESR Cap model versus ABAQUS cap model (L cycle data)	17
Figure 6	Measured versus predicted uniaxial strain response (L cycle runs)	17
Figure 7	ESR Cap model versus ABAQUS cap model (G cycle data)	19
Figure 8	Measured versus predicted uniaxial strain response (G cycle runs)	19
Figure 9	ESR Cap model versus ABAQUS cap model (H cycle data)	21
Figure 10	Measured versus predicted uniaxial strain response (H cycle runs)	21
Figure 11	Measured versus predicted shear failure (I cycle)	23
Figure 12	Measured versus predicted uniaxial strain response (I cycle)	23
Figure 13	ESR Cap model versus ABAQUS cap model (K cycle data)	25
Figure 14	Measured versus predicted uniaxial strain response (K cycle)	25
Figure 15	ESR Cap model versus ABAQUS cap model (L cycle data)	27
Figure 16	Measured versus predicted uniaxial strain response (L cycle)	27

This page intentionally left blank.

Tables

Table 1	Layer J Diatomite Parameter Values for the ABAQUS Model	13
Table 2	Layer J Diatomite Parameter Values for the ESR Model	14
Table 3	Layer M Diatomite Parameter Values for ABAQUS Model	16
Table 4	Layer M Diatomite Parameter Values for ESR Model	16
Table 5	Layer G Diatomite Parameter Values for ABAQUS Model	18
Table 6	Layer G Diatomite Parameter Values for ESR Model	18
Table 7	Layer H Diatomite Parameter Values for ABAQUS Model	20
Table 8	Layer H Diatomite Parameter Values for ESR Model	20
Table 9	Layer I Diatomite Parameter Values for ABAQUS Model	22
Table 10	Layer I Diatomite Parameter Values for ESR Model	22
Table 11	Layer K Diatomite Parameter Values for ABAQUS Model	24
Table 12	Layer K Diatomite Parameter Values for ESR Model	24
Table 13	Layer L Diatomite Parameter Values for ABAQUS Model	26
Table 14	Layer L Diatomite Parameter Values for ESR Model	26

This page intentionally left blank.

Introduction

In 1994 a cooperative national laboratory/industry research program was initiated to improve understanding of the geomechanical processes causing well casing damage during oil production from weak, compactible formations. The program focuses on the shallow diatomaceous oil reservoirs located in California's San Joaquin Valley, and combines analyses of historical field data, experimental determination of rock mechanical behavior, and geomechanical simulation of the reservoir and overburden response to production and injection. A comprehensive database, consisting of historical well failure, production, injection, and subsidence data was compiled to provide a unique and complete picture of the reservoir and overburden behavior at the Belridge Diatomite Field (Myer et al., 1996, Fredrich et al., 1996). Analyses of the field-wide data base indicated that two-dimensional (plane-strain) geomechanical simulations could not capture the locally complex production, injection, and subsidence patterns, and motivated large-scale, three-dimensional geomechanical simulations (Fredrich et al., 1996, 1998).

Sandia National Laboratories' quasi-static, large-deformation structural mechanics finite element code, JAS3D, was used to perform the three-dimensional geomechanical simulations (Fredrich et al., 1996, 1998). JAS3D provides several constitutive models to simulate time-independent elastic or inelastic (non-linear) deformation as well as time-dependent (creep) behavior. One of these material models, referred to herein as the Extended Sandler-Rubin (ESR) Cap Model (Fossum, 1998) is a generalized version of the Sandler and Rubin cap plasticity model (Sandler and Rubin, 1979). The ESR Cap Model includes a smooth, three-stress-invariant composite yield surface comprising a shear failure surface with an option for nonassociative flow, and a hardening/softening yield surface (cap) to account for inelastic compaction at stress states below the shear surface.

The ESR Cap Model is qualitatively similar to the cap model implemented in the commercial finite element code ABAQUS (Hibbit, Karlsson & Sorensen, Inc.) that was used by Shell E&P in earlier two-dimensional finite element modeling of the Belridge Diatomite Field (de Rouffignac et al., 1995). However, there are several notable differences between the two models. In the current context, the most significant difference is that the ESR Cap Model includes a non-linear shear failure surface whereas the shear failure surface in the ABAQUS Cap Model is constrained to be linear.

Initially, a baseline three-dimensional geomechanical simulation using Sandia's JAS3D code was performed that employed a Drucker-Prager material model for the reservoir rock (Fredrich et al., 1996). Subsequently, the ESR Cap Model was implemented in JAS3D and used to describe the reservoir rock (Fredrich et al., 1998). Initially, the constitutive parameters for the ESR Cap Model were determined by generating "synthetic" data sets from the material model parameters used in Shell's previous two-dimensional finite element modeling (de Rouffignac et al., 1995), and then deriving the ESR Cap Model parameters from the resultant "synthetic" data sets. This constrained the ESR Cap Model to be identical to the ABAQUS Cap Model for the particular set of constitutive parameters derived (see Fredrich et al. (1996) for these parameter values).

In the spring of 1996, CalResources LLC (now known as Aera Energy LLC) requested that Sandia National Laboratories consider Shell E&P's original experimental data (in so far as it was

available) and re-derive the constitutive parameters for the ESR Cap Model directly from the experimental data. The newly derived constitutive parameters would be used in additional geomechanical simulations performed at Sandia and in future simulations to be performed at Shell E&P Tech. Co. (e.g., Fredrich et al., 1998). This report documents the experimental rock mechanics data and constitutive material models that were derived to describe the Belridge Diatomite reservoir rock.

General Description of Belridge Diatomite Reservoir

The Belridge Field is developed on two elongated northwestward-trending anticlines that are structurally offset by the Middle Belridge fault. The field contains two hydrocarbon reservoirs that are produced independently of one another: the diatomite (as used here, this includes both diatomite and porcelanite lithologies), and the overlying Tulare.

The diatomite reservoir produces 10-34° gravity oil from depths of about 800 to 3000 feet, depending upon structural position. The diatomite is a biogenic siliceous deposit consisting of the shells or tests of diatoms with varying amounts of detrital material (principally clay and sand) so that individual depositional cycles are identifiable, with the rock ranging from fairly pure to shaley diatomite. In the upper intervals, diatoms are preserved as opal-A, which is an amorphous, colloidal form of silica. Porosity ranges from 50-70%. With increasing depth (pressure) and temperature, the mineralogic phase changes from opal-A to opal-CT. The associated reduction in porosity (<45%) makes the diatomite reservoir significantly less productive below the opal-CT transition. Below this, the diatom skeletal structures are no longer well preserved and the rock is a porcelanite.

The diatomite is unconformably overlain by the Plio-Pleistocene-aged Tulare Formation on the crest and by the Pliocene-aged Etchegoin and San Joaquin Formations on the flanks. The Tulare is the second reservoir at Belridge and produces 11-14° gravity oil from multiple, highly discontinuous reservoir sands totaling about 400-1500 feet in thickness. Overlying the Tulare is 100-200 feet of unsaturated alluvium.

A detailed description of the reservoir model used for the three-dimensional fluid flow and geomechanical simulations is given in Fredrich et al. (1996, 1998).

Description of ESR and ABAQUS Cap Models

The ESR and ABAQUS Cap Models are similar in that each attempts to describe the same phenomenological behavior, but they differ in the mathematical description of the phenomena:

Similarities

1. Both models use a nonhardening shear failure surface that can accommodate differences in shear strength between triaxial extension and triaxial compression.
2. Both models can invoke a nonassociative flow rule to model dilatant strains more accurately.
3. Both models use associated flow in the cap region.
4. Both models use an elliptically shaped hardening cap that, analogous to the shear failure surface, can accommodate differences in cap yield and hardening behavior between triaxial extension and triaxial compression.

5. Both models can model transient time dependent behavior if specified.

Differences

1. The ABAQUS model uses a linear function to model the shear failure surface while the ESR Model uses an exponential function.
2. The ABAQUS model requires the user to input pressure-volume data and then linearly interpolates between data pairs to represent cap hardening while the ESR Model uses a functional representation of hardening and requires the user to input the necessary material constants.
3. The ABAQUS model uses a circular transition region between the shear failure surface and the cap surface while the ESR Model requires the cap surface to intersect the shear failure surface at the point the material is incompressible, i.e., isochoric (the so-called critical state).
4. The ESR Model will allow the cap surface to retract (soften) to model soil behavior more accurately. It is not clear from the ABAQUS manual whether or not the ABAQUS cap is allowed to soften.
5. The ESR Model has the option for the user to impose a limited tension or tension cut-off while the ABAQUS model does not provide for a tension cut-off.
6. Mathematically, the ABAQUS model writes the shear failure and cap yield criteria in terms of the stress invariants $\sqrt{3J_2}$ and $I_1/3$ while the ESR Model uses $\sqrt{J_2}$ and I_1 .

Mathematical Description of the ESR Cap Model

The ESR Cap Model generalizes the soil and rock constitutive model of Sandler and Rubin (1979) by incorporating Lode-angle dependence of yield in the deviatoric plane and nonassociativity in the meridional plane on the shear yield (failure) surface. Cap deformation is always associative. The model is designed to represent the elastic-plastic behavior of porous rock and soil. The model includes a nonlinear, nonhardening shear yield surface that varies with Lode angle, and a hardening or softening cap as illustrated in Figure 1. Linear elastic behavior occurs when the stress point is within the composite shear-failure and yield-cap surfaces.

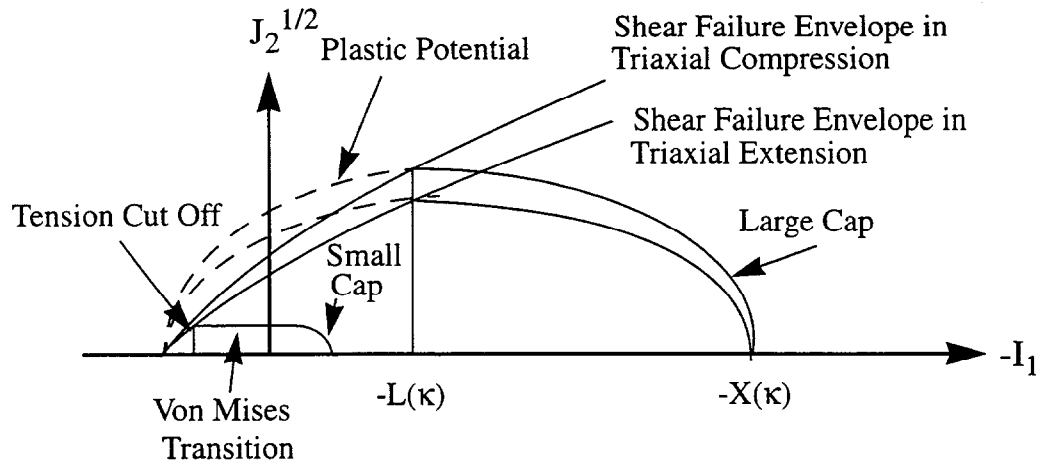


Figure 1. Composite yield surface representation for the ESR Cap plasticity model.

When the stress point lies on the shear failure envelope, shear failure occurs according to the yield function,

$$F_s = \Gamma \sqrt{J_2} - A + C \exp(BI_1) \quad (1)$$

where J_2 is the second invariant of the deviator stress, I_1 is the first invariant of the Cauchy stress, A , B , and C are material constants. Γ is a function of J_3 , the third invariant of the deviator stress that incorporates the Lode-angle dependence of yield, and is given by

$$\Gamma = \frac{1}{2} \left\{ [1 + \sin(3\psi)] + \frac{1}{K} [1 - \sin(3\psi)] \right\} \quad (2)$$

where K is the ratio of the yield stress in triaxial extension to the yield stress in triaxial compression. ψ is the Lode angle given by

$$\psi = \frac{1}{3} \arcsin \left(-\frac{27}{2} \frac{J_3}{(3J_2)^{3/2}} \right) \quad -\frac{\pi}{6} \leq \psi \leq \frac{\pi}{6} \quad (3)$$

where for triaxial extension, $\psi = -\pi/6$, and for triaxial compression, $\psi = \pi/6$. Note that for triaxial compression, $\Gamma = 1$, while for triaxial extension, $\Gamma = 1/K$. Thus, the difference in strength between triaxial compression and triaxial extension stress states in this formulation is handled by multiplying the loading variable, $\sqrt{J_2}$, by a factor Γ such that the yield function experiences an apparent higher loading condition for stress states different from triaxial compression, depending on the value of J_3 . An alternative to this approach would be to modify the strength directly. However, since the Lode angle, ψ , is independent of deviatoric stress scaling, it is convenient to use the former formulation in a modified radial return integration algorithm.

When the stress point lies on the cap and pushes it outward, plastic strain comprises an irreversible decrease in volume called compaction, and a shear component for non-hydrostatic compression stress states. The cap motion is related to the plastic decrease in volume through a hardening rule. The shape of the cap is described as an elliptical surface defined by

$$\Gamma \sqrt{J_2} = \frac{1}{R} \sqrt{[X(\kappa) - L(\kappa)]^2 - [I_1 - L(\kappa)]^2} \quad (4)$$

in which

$$L(\kappa) = \begin{cases} \kappa & \text{if } \kappa < 0 \\ 0 & \text{if } \kappa \geq 0 \end{cases} \quad (5)$$

$$X(\kappa) = \kappa - R[A - C \exp(BL)] \quad (6)$$

The cap position parameters $L(\kappa)$ and $X(\kappa)$ locate the current cap surface. The material parameter, R , defines the ratio of principal ellipse radii of the cap surface. The hardening parameter, κ , is defined through a functional of $X(\kappa)$ and volumetric plastic strain, ϵ_v^p , caused only by cap action,

$$\bar{\epsilon}_v^p = W[\exp\{D_1(X - X_0) - D_2(X - X_0)^2\} - 1] \quad (7)$$

in which W , D_1 , and D_2 are material parameters, X_0 is the initial cap position, and $\bar{\epsilon}_v^p$ is a history-dependent functional of ϵ_v^p given by

$$\dot{\bar{\epsilon}}_v^p \equiv \min(\dot{\epsilon}_v^p, 0) \quad (8)$$

Sandler and Rubin (1979) introduced this condition to prevent the cap from retracting for rock behavior. The cap is allowed to retract for soil behavior.

A limited tension, or tension cut off, option is also available in the model as illustrated in Figure 1. The user inputs this value in terms of a positive value of I_1 .

The cap intersects the shear failure surface at the point on the cap with zero horizontal tangency, i.e., the point of zero dilatancy. When the cap is too small to intersect the shear failure surface, the point of horizontal tangency on the cap is extended as a Von Mises surface until either the shear failure or tension cut off surface is intersected.

In the nonassociative case, the plastic potential takes the form of an ellipse as illustrated in Figure 1. The functional form of this potential is given by

$$G_s = \Gamma \sqrt{J_2} - \frac{[L(\kappa) - X(\kappa)]}{R \left[\frac{1}{B} \ln \left(\frac{A}{C} \right) - L(\kappa) \right]} \sqrt{\left[\frac{1}{B} \ln \left(\frac{A}{C} \right) - L(\kappa) \right]^2 - [I_1 - L(\kappa)]^2} \quad (9)$$

A procedure for estimating the parameters for this class of cap models is given in Fossum et al. (1995).

If an initial volumetric compaction strain is specified at the beginning of an analysis, the corresponding state variable, L , must be updated. If, in addition, an initial stress field is specified, the corresponding state variable, L , and the volumetric compaction strain must be updated as necessary.

Constitutive Models for Belridge Diatomite

Experimental Data Provided by Shell E&P Tech. Co.

The experimental data used in this work were contained in seven QUATTROPRO (Novell, Inc.) spreadsheets and consist of conventional triaxial compression strength data for six cycles of diatomite (G, H, J, K, L, and M) and uniaxial strain data for three of the cycles (G, J, and M). A detailed description of the reservoir geology and cyclic nature of the diatomite reservoir rock is given in Fredrich et al. (1996, 1998).

Constitutive Parameter Estimation

The shear failure parameters were determined by a variant of the Levenberg-Marquardt Optimization Method (Fossum, 1995, 1997), while the cap parameters were determined by direct simulation in which the cap parameters were varied until an acceptable fit was obtained. Because of a lack of data, the cap parameters for cycles H, K, and L were selected based on a significant amount of engineering judgement.

In general, all the data are sparse. The most serious deficiency in the shear failure data is lack of data, particularly for tensile stress states and low values of mean stress. In some cases, a nonlinear fit to the data indicates that the material exhibits negligible (and in some cases, negative) cohesion (Cycles J & M) and a negative internal friction angle (Cycle J). In another case (Cycle H) the material shows extreme variability. Additional unconfined compression tests and indirect tensile tests should be performed for all cycles, and the repeatability of the data for all cycles should be established.

Uniaxial strain data are incomplete in the following ways:

- data do not exist for four of the seven cycles;
- only one stress component is provided for the remaining three cycles; and
- data for two of the three cycles (Cycles G & M) end prematurely at very low strains (< 5%),

i.e., before lock-up is indicated.

It would be desirable to conduct uniaxial strain tests similar to the three performed for Cycle J to strains of 15-25%. Additionally, in the spreadsheets provided for Cycles J & M, offset strains were introduced by extrapolating the data to an assumed yield stress, subtracting the measured strains to this point, and then adding the estimated corresponding elastic strains. This was likely done because of poor strain resolution in the initial seating and load-up stages of the experiment. However, this procedure was not followed for Cycle G.

Cycle J

Shear Failure

Data were provided as follows:

1. Well # 526L-34 Depth 1314 ft. Interval J top
2. Well # 533E-29 Depth 1414 ft. Interval J top
3. Well # 754N-33 Depth 1241 ft. Interval J bot
4. Well # 754N-33 Depth 1242 ft. Interval J bot

Data from No. 2 give unrealistic strength values (negative values of shear strength for mean stresses less than about 220 psi), and data from No. 3 show a decrease in shear strength with increasing mean stress. Thus only the eleven data points from Nos.1 and 4 were used in the parameter estimation.

The fitted ESR Model shows near linear shear strength behavior as a function of I_1 between I_1 values of 0 and 250 psi, followed by strongly nonlinear behavior between I_1 values of 250 and 2500 psi. After 2500 psi the shear strength is nearly independent of I_1 . The model also predicts negligible cohesion. Additional failure data would be desirable between I_1 values of 0 and 1000 psi (mean stresses between 0 and 350 psi).

Cap Action

Axial stress versus axial strain data were provided from six isothermal uniaxial strain tests. No confining pressure data were available. All but one of the tests exceeded 5 percent strain and three of the tests exceeded 25 percent strain.

The offset strains originally provided by Shell were used in the fitting process. To capture the curvature of the stress-strain data, the isotropic cap hardening function was modified to incorporate one additional material constant. The cap hardening parameter, κ , used originally in the DOE-sponsored well failure project (see Fredrich et al., 1996) was defined by a functional of the cap position parameter $X(\kappa)$ and the plastic volumetric strain caused by cap motion,

$$\bar{\epsilon}_v^p = W[\exp\{D(X - X_0)\} - 1] \quad (10)$$

where W and D are material parameters. This was modified to

$$\bar{\epsilon}_v^p = W[\exp\{D_1(X - X_0) - D_2(X - X_0)^2\} - 1] \quad (11)$$

where now there are two material parameters, D_1 , and D_2 , in the exponential term. The SNL model accurately predicts the measured stress to 35 percent strain. Data appear to be sufficient to define the cap parameters accurately.

Cycle M

Shear Failure

Data were provided as follows:

1. Well # 533E-29 Depth 1812 ft. Interval M middle

No unconfined compression data were provided and the lowest I_1 value was 1410 psi. In all, 5 data points were used in the parameter estimation. The fitted model shows modest nonlinearity over a range in I_1 of 0 to 5500 psi and predicts negligible cohesion. Additional failure data would be desirable between I_1 values of 0 and 1000 psi (mean stresses between 0 and 350 psi).

Cap Action

Axial stress versus uniaxial strain data were provided from eight isothermal uniaxial strain tests. No confining pressure data were available. All of the tests terminated between approximately one and three percent strain. In general the tests showed good repeatability; however, run 87 showed a significant departure from the others (even including its elastic behavior, possibly indicating an incompetent specimen), and thus was not used in the fitting procedure.

The offset strains originally provided by Shell were used in the fitting process. The original SNL model, i.e., the original cap hardening function, was adequate in defining the curvature of the stress-strain behavior (i.e., the best fit yielded $D_2 = 0.0$). This is probably an artifact of the very limited strains achieved in this test.

Cycle G

Shear Failure

Data were provided as follows:

1. Well # 533E-29 Depth 785 ft. Interval G top

2. Well # 43L015-29 (no other information provided)

In all, 8 data points were used in the parameter estimation. No unconfined compressive strengths were provided. The fitted model shows moderate nonlinearity for I_1 values between 0 and 3000 psi and a non-zero cohesion.

Cap Action

Axial stress versus axial strain data were provided from two isothermal uniaxial strain tests. Both tests terminated before 5 percent strain was reached. No confining pressure data were available. Additionally no offset strain data were available. Model fits were attempted using both the raw data provided and with assumed offset strains calculated in a manner identical to that used for cycles J and M. In either case, the best fit indicates that pore collapse initiates upon application of any load (note that for comparison, the cap position has been hardened in the figure showing the ESR Cap Model versus the ABAQUS Cap Model for G cycle data). Additional uniaxial strain tests for this layer are recommended.

Cycle H

Shear Failure

Data were provided as follows:

1. Well # 526L-34 Depth 1064 ft. Interval H top

In all, only 3 data points were available for parameter estimation. The data show significant scatter. No unconfined compressive strengths were provided. The best fit, using the exponential SNL model, predicts linear behavior. Additional triaxial compression data are required to define the failure surface adequately.

Cap Action

No uniaxial strain data were provided. The uniaxial strain tests from cycle G were used for this cycle because the shear failure data at moderate values of I_1 (~3000 psi) from cycle G more closely matched the shear failure data from cycle H than that from cycles J or M. However, the shear failure surface at lower values of I_1 (~1000 psi) is not similar to that of any of the cycles, including G. Uniaxial strain tests are required to evaluate the cap parameters for this cycle adequately.

Cycle I

Shear Failure

No shear data were provided for this cycle. The original shear failure parameters for the I cycle were obtained by averaging the shear failure data for the H and J cycles. The revised shear failure parameters were obtained by fitting the ESR Cap Model to the shear failure data of cycles H and

J. The applicability of these data to cycle I is uncertain and triaxial compression data are required to define the failure surface adequately.

Cap Action

No uniaxial strain data were provided. The original cap parameters were derived from the uniaxial strain data for the J cycle. The revised cap parameters were obtained through simulation using the ESR Cap Model and the uniaxial strain data for cycles J and G. The applicability of these data to cycle I is uncertain and uniaxial strain tests are required to evaluate the cap parameters adequately.

Cycle K

Shear Failure

Data were provided as follows:

1. Well # 754N-33 Depth 1296 ft. Interval K top

In all, 4 data points were available for parameter estimation, including one from an unconfined compression test. The fitted model shows moderate nonlinearity for I_1 values to 2500 psi with a non-zero value for cohesion. Shear failure is reasonably well characterized.

Cap Action

No uniaxial strain data were provided. The uniaxial strain tests from cycle M were used for this cycle because the shear failure data from cycle M were *somewhat* more similar to the shear failure data from cycle K than that from cycles J or G. The extrapolation of cap parameters for this cycle is approximate and uniaxial strain tests are required to evaluate the cap parameters adequately.

Cycle L

Shear Failure

Data were provided as follows:

1. Well # 754N-33 Depth 1444 ft. Interval L bot
2. Well # 754N-33 Depth 1449 ft. Interval L bot

In all, 8 data points were available for parameter estimation, including one from an unconfined compression test. The fitted model shows moderate nonlinearity for I_1 values to 3500 psi and a non-zero cohesion.

Cap Action

No uniaxial strain data were provided. The uniaxial strain tests from cycle M were used for this cycle because the shear failure data from cycle M more closely matched the shear failure data from

cycle L than that from cycles J or G. Uniaxial strain tests are required to evaluate the cap parameters adequately.

Summary Remarks on Experimental Data

The triaxial compression and uniaxial strain data varied in their completeness as noted below:

- No triaxial data were provided for the I cycle. Following E.P. de Rouffignac (personal communication, 1996), the shear failure parameters for the I cycle were obtained by averaging the shear failure data for the H and J cycles. The cap parameters were derived from the uniaxial strain data for the J cycle. The validity of the constitutive parameters derived for the I cycle is therefore less certain.
- Triaxial strength data provided for the H cycle indicate substantial scatter that therefore introduces substantial uncertainty into the constitutive parameters derived for the shear failure surface for this cycle.
- The fit to the shear failure surface for several of the cycles (H, K, L, M) would be better constrained with additional data at low stresses. Fits for all cycles would be more robust with the inclusion of tensile strength data since the available data indicate that the failure envelope exhibits large curvature at low stresses.
- The uniaxial strain tests were conducted in an oedometer cell. Axial stress was measured using an external load cell. Axial displacement of the test specimen was likewise measured external to the vessel, and then corrected for elastic displacement of the intervening elements of the loading column. External measurements of stress and strain are less accurate than direct internal measurement, and are typically subject to high uncertainties at low loads. It is suspected that this is the origin of a zero offset originally applied to the experimental data by Shell E&P Tech. Co. Also, in an oedometer cell, the uniaxial strain condition is only approximately satisfied. The sample is constrained from deforming in the radial directions by containment in a rigid vessel, which is not infinitely rigid. Furthermore, friction along the vessel-sample interface may perturb the state of stress and therefore alter the material response. Friction along the interface also reduces the true axial load supported by sample. It was understood that the experimental data as originally provided were corrected for friction, but the details of this correction were not provided.
- Uniaxial strain data were provided for only three cycles of the diatomite (G, J, and M). In addition, the tests were not conducted to as large axial strains as would be desirable for two of the three cycles for which data were provided (G and M).
- Fits to the constitutive parameters for the cap yield surface for those cycles for which uniaxial strain data were unavailable are less valid. The decision as to which uniaxial strain data to use (G, J, or M) for each of the cycles for which no data were available (H, I, K, and L) was based on similarities in the overall level and shape of the shear failure surface. Cycle G uniaxial data were used to derive cap parameters for cycle H because the cycle H triaxial data suggested relative hardening at higher stresses (I1 ~3000 psi) similar to that exhibited by cycle G,

whereas the cycle J data suggested less hardening at these pressures. The cap yield surface for cycle K was fitted using uniaxial strain data for cycle M; however, it is noteworthy that there was not any strongly compelling reason for the use of the cycle M versus cycle J data. Finally, the cap parameters for cycle L were derived using uniaxial strain data for cycle M because the overall level of the shear failure envelope for cycle L was more comparable to that for cycle M than that for either cycles G or J. However, the shear failure surfaces for cycles L and M are only crudely similar.

- Available data from the uniaxial strain tests includes only axial strain and total axial stress . The radial (confining) stress was not provided. The constitutive model would be better constrained if both axial stress and confining pressure were known.

Constitutive Parameters and Comparative Plots

Tables 1-14 give a compilation of the constitutive parameters accompanied by Figures 2-16 that show the shear failure data used in the fitting, the revised ESR Cap Model shear failure predictions versus the original ABAQUS model predictions, and the measured versus predicted uniaxial strain response using the ESR Cap Model.

Table 1: Layer J Diatomite Parameter Values for the ABAQUS Model

Parameter	Value
Bulk Modulus	33,333.0 psi
2G	50,000.0 psi
d	174.0 psi
β	40.1 degrees
R	0.3
α	0.01
K	1.0
Hardening	(psi)
0.0	54.0
0.009	200.0
0.022	400.0
0.13	900.0
0.14	1200.0

Table 2: Layer J Diatomite Parameter Values for the ESR Model

Parameter	Value
Bulk Modulus	33,333.0 psi
2G	50,000.0 psi
A	394.4 psi
B	1.869E-03 1/psi
C	393.8 psi
D ₁	5.0E-05 1/psi
D ₂	1.7E-07 1/psi ²
R	1.559
W	0.21
X ₀	-200.0 psi
TCUT	None
LTYPE	2.0
K	1.0 (No Lode angle dependence)
ASSOC	0 (Associative)
INITIAL COMPACTION	None

Figure 2. ESR Cap Model versus ABAQUS Cap Model (J cycle data)

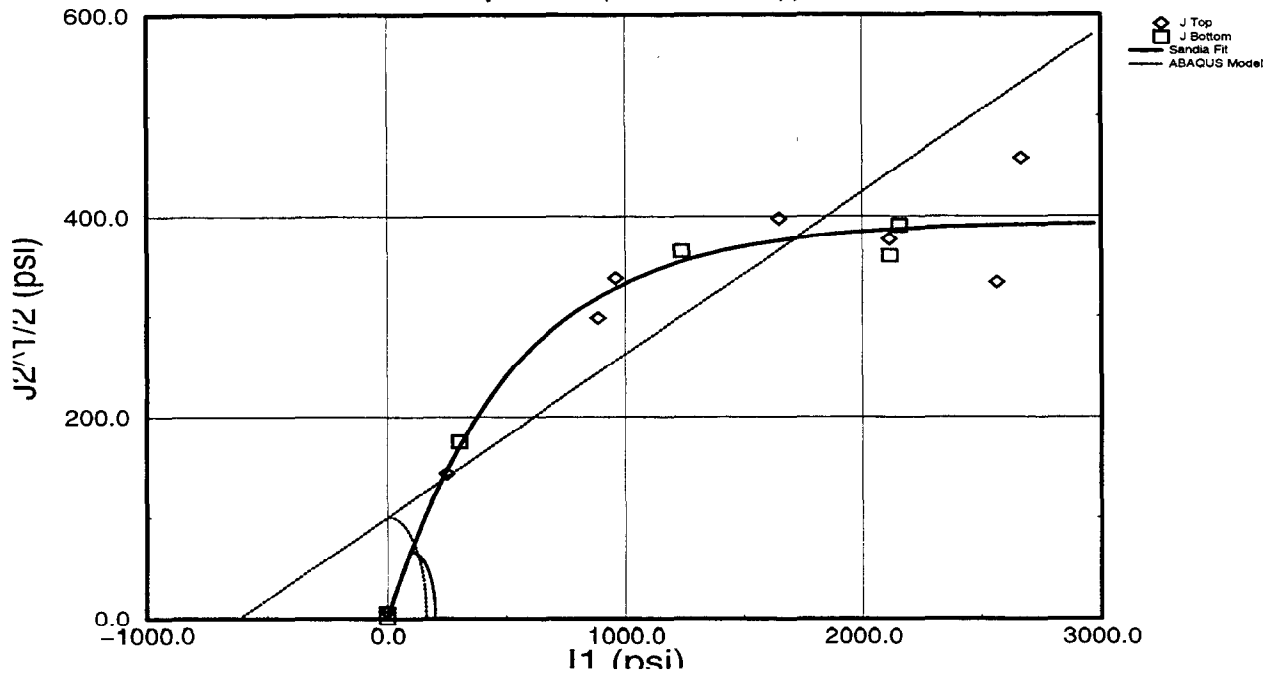


Figure 3. Measured versus predicted uniaxial strain response (J cycle runs)

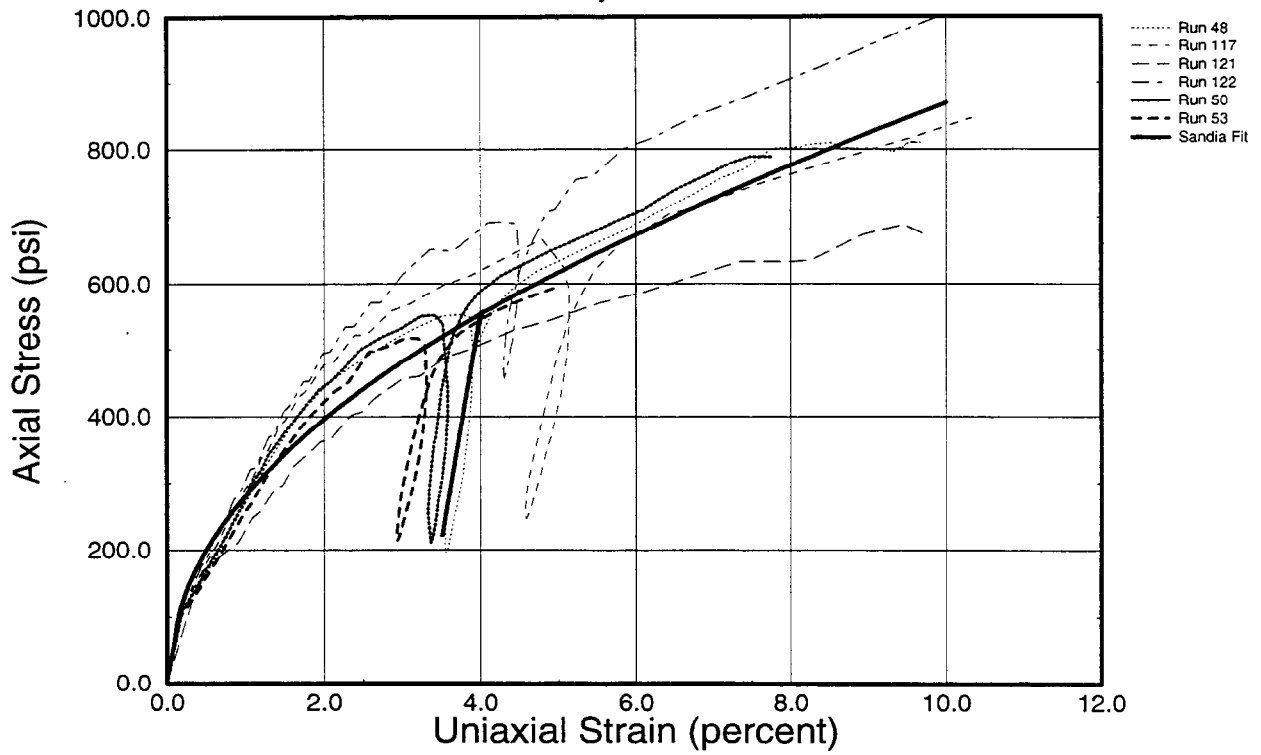


Figure 4. Measured versus predicted uniaxial strain response (J cycle runs)

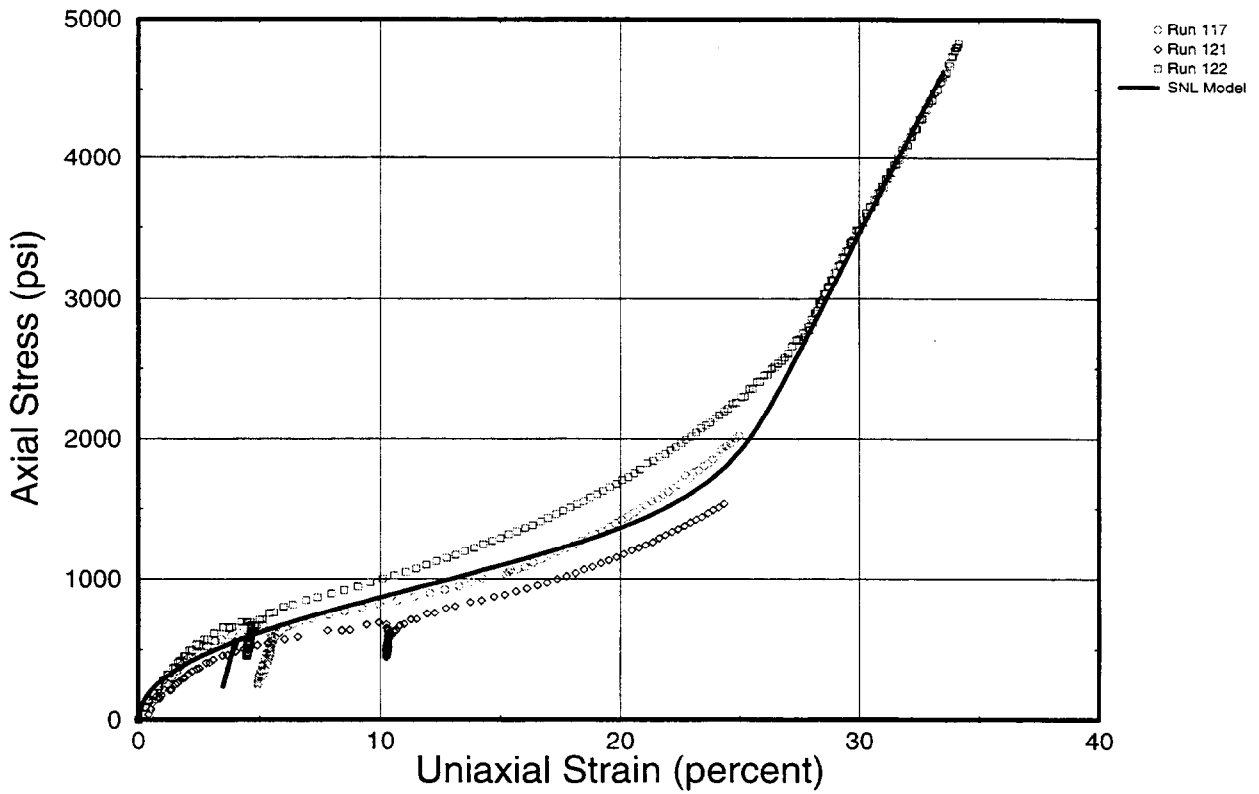


Table 3: Layer M Diatomite Parameter Values for ABAQUS Model

Parameter	Value
Bulk Modulus	82,121 psi
2G	138,974 psi
d	247.0 psi
β	58.5 degrees
R	0.23
α	0.01
K	1.0
Hardening	(psi)
0.0	61.0
0.00236	200.0
0.0055	600.0
0.012	1100.0
0.02	1400.0

Table 4: Layer M Diatomite Parameter Values for ESR Model

Parameter	Value
Bulk Modulus	82,121.0 psi
2G	138,974.0 psi
A	4,252.2 psi
B	1.062E-04 1/psi
C	4,252.0 psi
D ₁	2.80E-05 1/psi
D ₂	0.0 1/psi ²
R	3.8
W	0.08
X ₀	- 183.0 psi
TCUT	None
LTYPE	2.0
K	1.0 (No Lode angle dependence)
ASSOC	0 (Associative)
INITIAL COMPACTION	None

Figure 5. ESR cap model versus ABAQUS cap model (L cycle data)

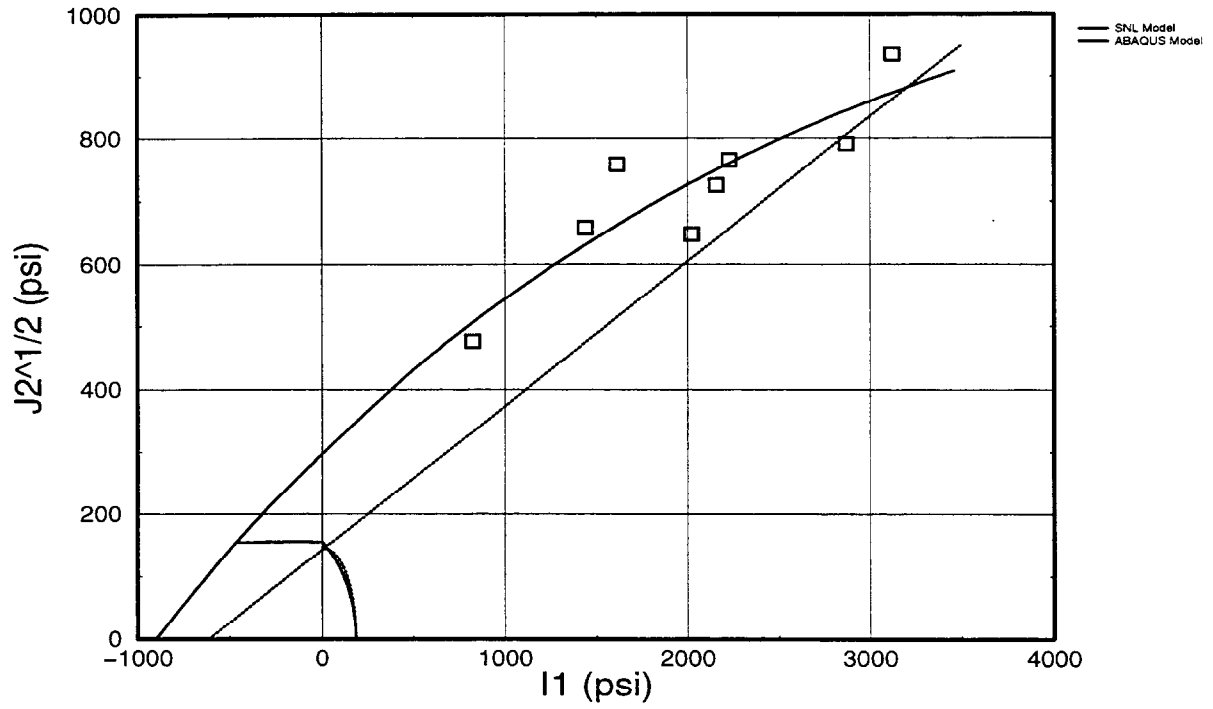


Figure 6. Measured versus predicted uniaxial strain response (L cycle runs)

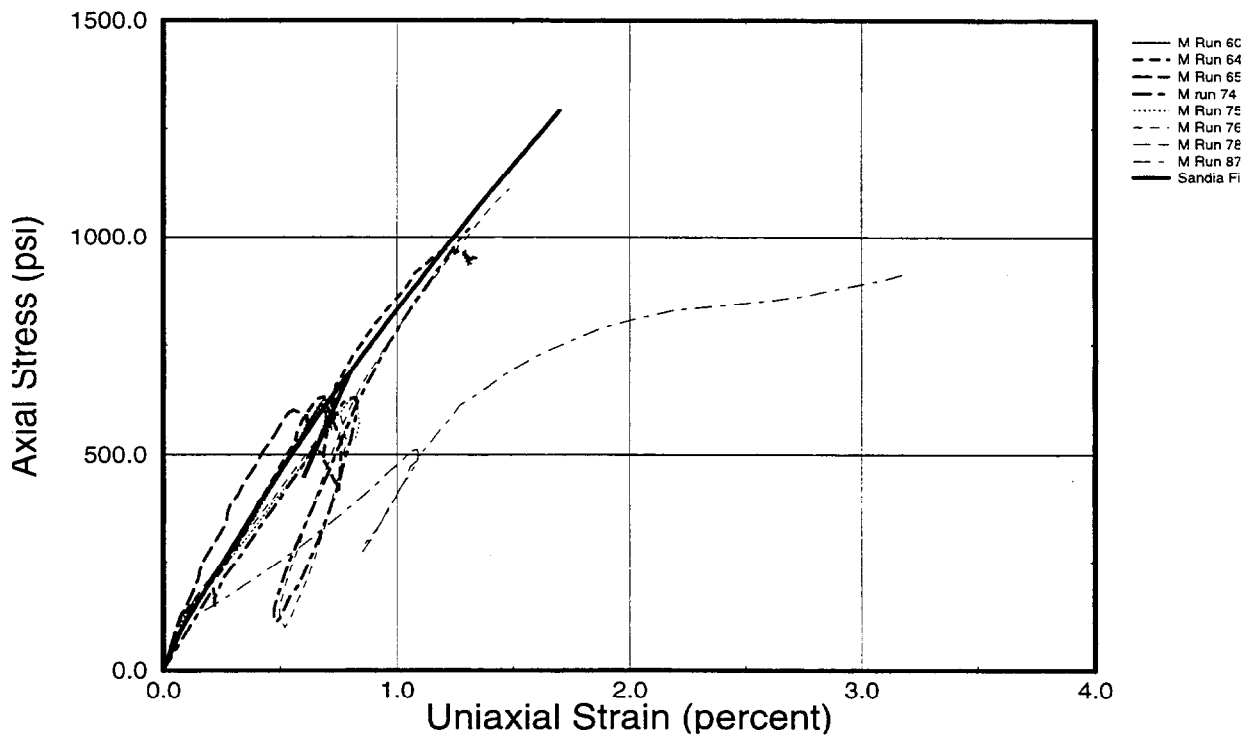


Table 5: Layer G Diatomite Parameter Values for ABAQUS Model

Parameter	Value
Bulk Modulus	24,090.0psi
2G	40,769.0 psi
d	200.0 psi
β	36.9 degrees
R	0.33
α	0.01
K	1.0
Hardening	(psi)
0.0	69.0
0.00712	200.0
0.015	400.0
0.055	800.0
0.065	900.0

Table 6: Layer G Diatomite Parameter Values for ESR Model

Parameter	Value
Bulk Modulus	24,090.0 psi
2G	40,769 psi
A	486.1 psi
B	7.11E-04 1/psi
C	410.4 psi
D ₁	0.0 1/psi
D ₂	9.0E-08 1/psi ²
R	3.0
W	0.12
X ₀	0.0 psi
TCUT	None
LTYPE	2.0
K	1.0 (No Lode angle dependence)
ASSOC	0 (Associative)
INITIAL COMPACTION	None

Figure 7. ESR cap model versus ABAQUS cap model (G cycle data)

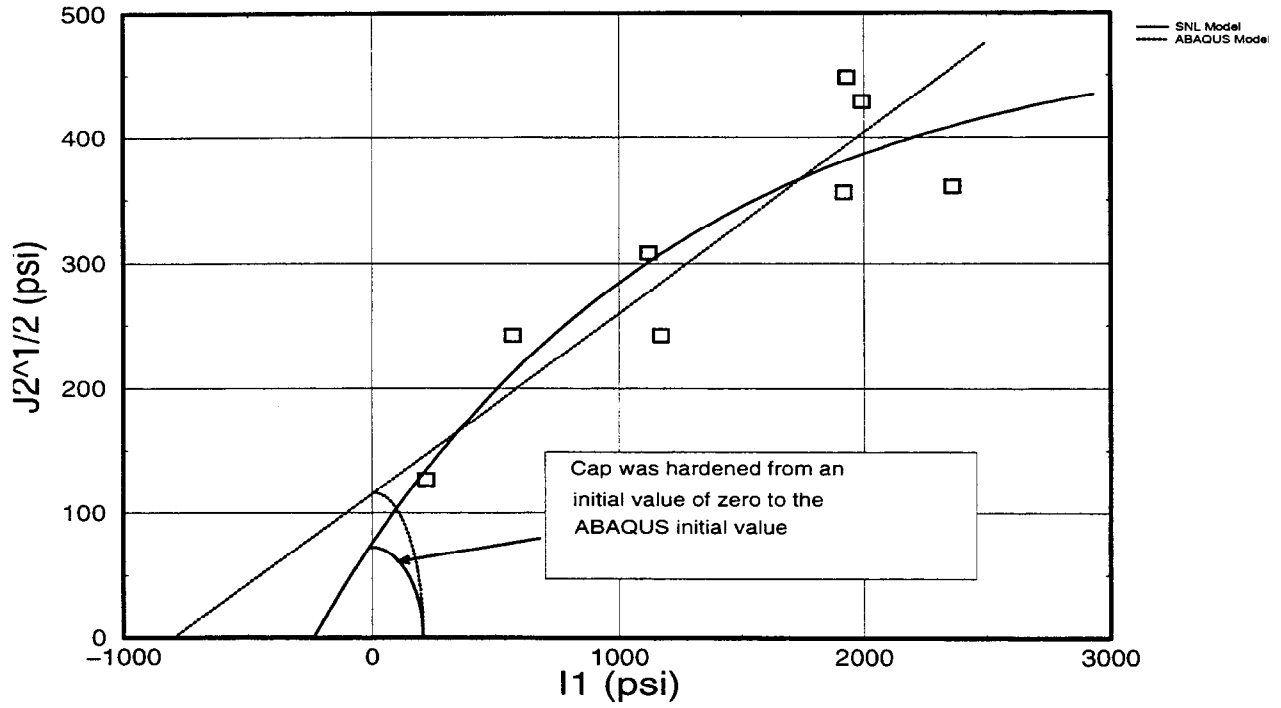


Figure 8. Measured versus predicted uniaxial strain response (G cycle runs)

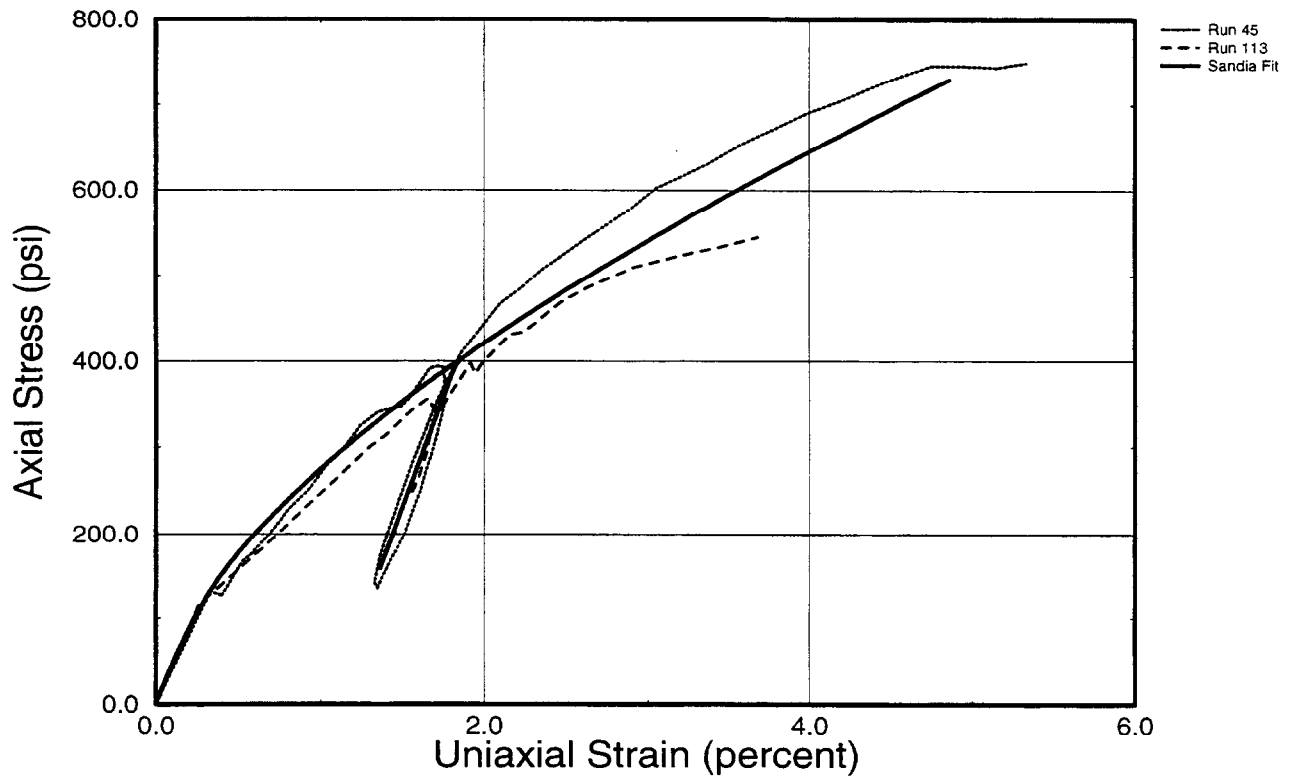


Table 7: Layer H Diatomite Parameter Values for ABAQUS Model

Parameter	Value
Bulk Modulus	31,818.0 psi
2G	53,846 psi
d	200.0 psi
β	39.4 degrees
R	0.33
α	0.01
K	1.0
Hardening	(psi)
0.0	69.0
0.0058	200.0
0.0125	400.0
0.0445	800.0
0.076	1000.0

Table 8: Layer H Diatomite Parameter Values for ESR Model

Parameter	Value
Bulk Modulus	31,818.0 psi
2G	53,846.0 psi
A	407032.4 psi
B	4.24E-07 1/psi
C	406887.9 psi
D ₁	0.0 1/psi
D ₂	9.0E-08 1/psi ²
R	4.5
W	0.12
X ₀	0.0 psi
TCUT	None
LTYPE	2.0
K	1.0 (No Lode angle dependence)
ASSOC	0 (Associative)
INITIAL COMPACTION	None

Figure 9. ESR cap model versus ABAQUS cap model (H cycle data)

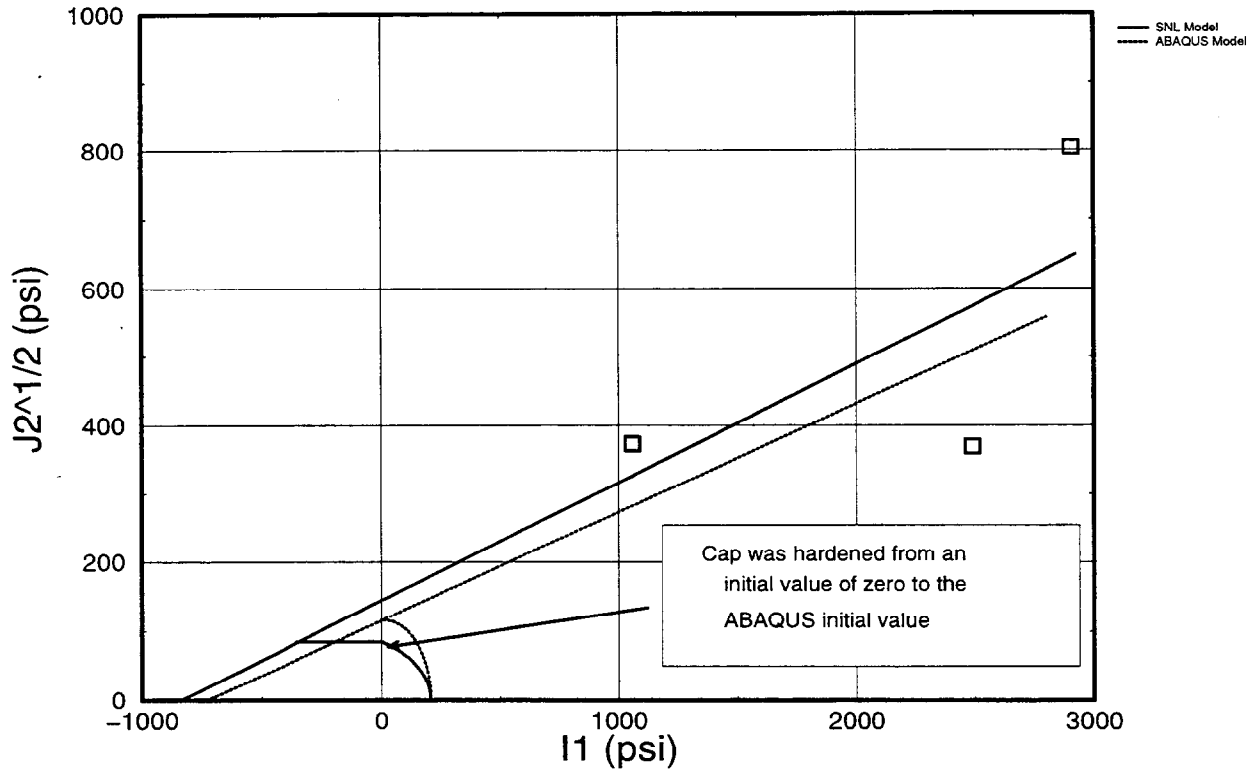


Figure 10. Measured versus predicted uniaxial strain response (H cycle runs)

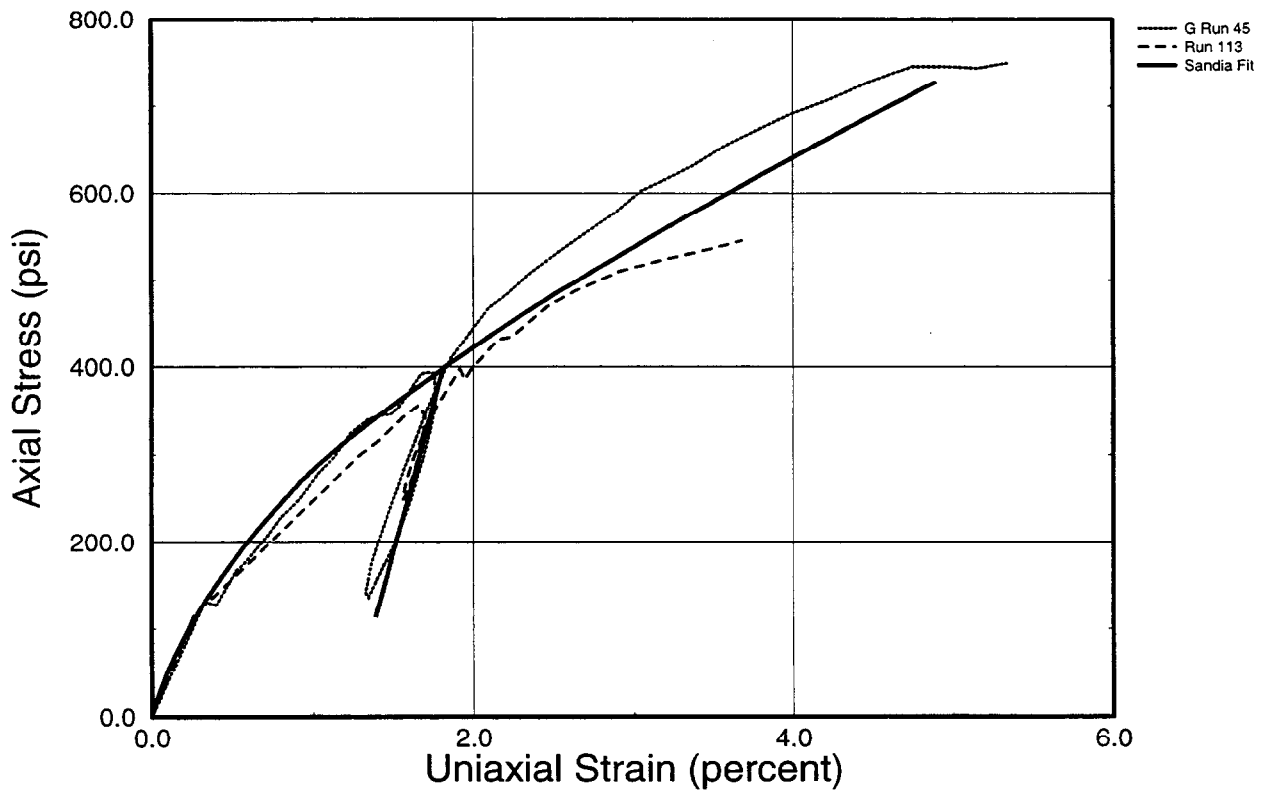


Table 9: Layer I Diatomite Parameter Values for ABAQUS Model

Parameter	Value
Bulk Modulus	42,580.0 psi
2G	66,554.0 psi
d	200.0 psi
β	42.0 degrees
R	0.34
α	0.01
K	1.0
Hardening	(psi)
0.0	71.0
0.005	200.0
0.0125	400.0
0.039	800.0
0.043	1000.0

Table 10: Layer I Diatomite Parameter Values for ESR Model

Parameter	Value
Bulk Modulus	32,576.0 psi
2G	51,923.0 psi
A	135,263.0 psi
B	9.19E-07 1/psi
C	135,100.0 psi
D ₁	2.50E-05 1/psi
D ₂	1.30E-07 1/psi ²
R	3.03
W	0.165
X ₀	-100.0 psi
TCUT	None (10,000 psi)
LTYPE	2.0
K	1.0 (No Lode angle dependence)
ASSOC	0 (Associative)
INITIAL COMPACTION	None

Figure 11. ESR cap model versus ABAQUS cap model (I cycle data)

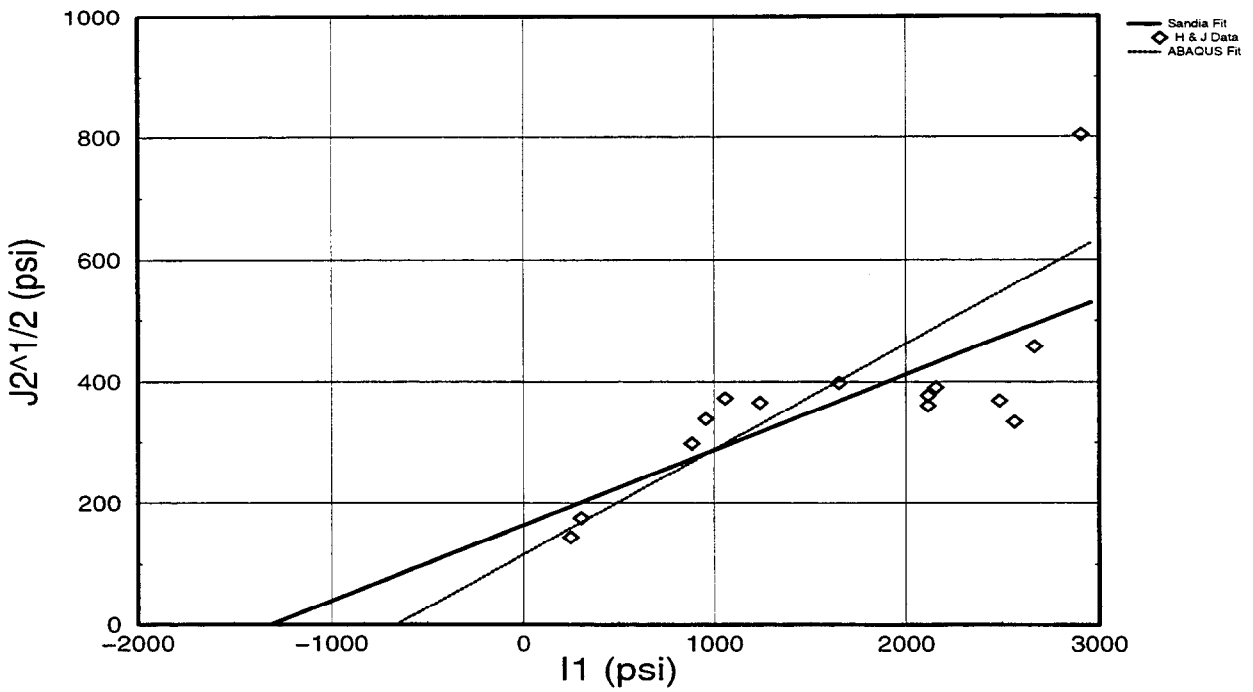


Figure 12. Measured versus predicted uniaxial strain response (I cycle runs)

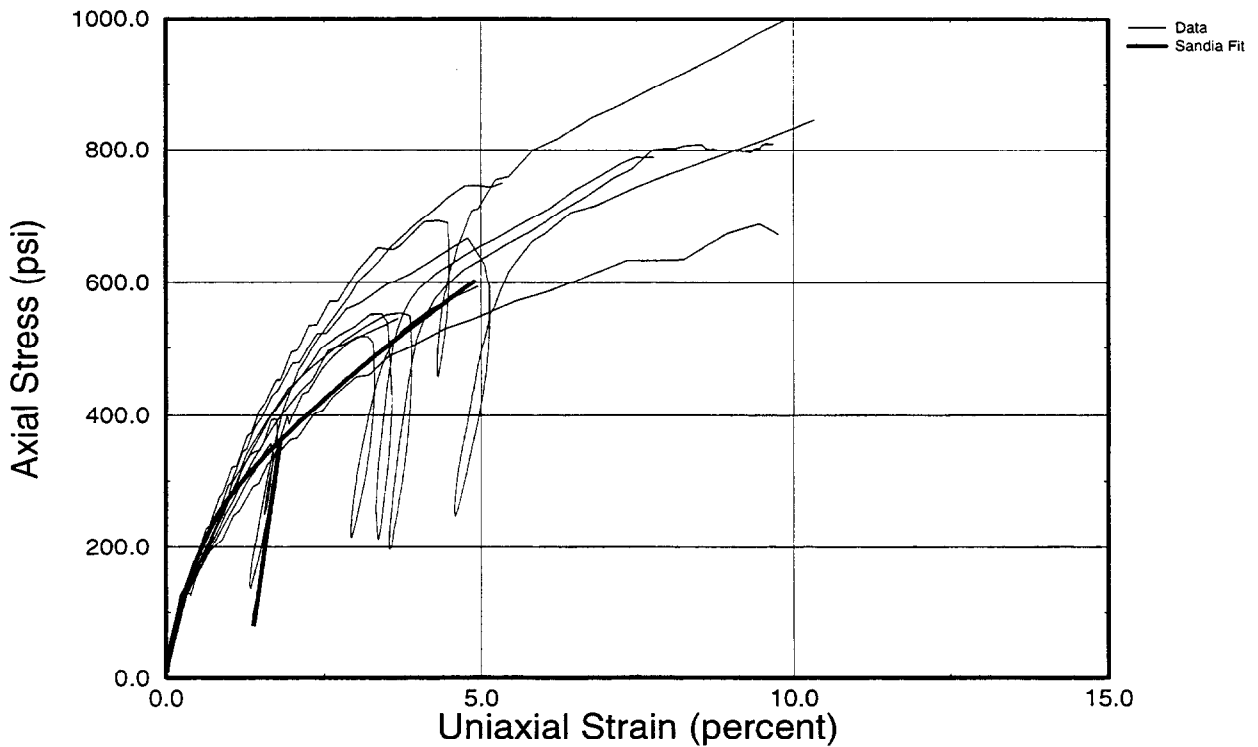


Table 11: Layer K Diatomite Parameter Values for ABAQUS Model

Parameter	Value
Bulk Modulus	36,161 psi
2G	61,196 psi
d	200.0 psi
β	40.4 degrees
R	0.3
α	0.01
K	1.0
Hardening	(psi)
0.0	62.0
0.0052	200.0
0.0066	400.0
0.0144	800.0
0.0205	1000.0
0.028	1200.0

Table 12: Layer K Diatomite Parameter Values for ESR Model

Parameter	Value
Bulk Modulus	36,161 psi
2G	61,196 psi
A	568.6 psi
B	8.61E-04 1/psi
C	444.0 psi
D ₁	1.0E-05 1/psi
D ₂	0.0 1/psi ²
R	1.4
w	0.05
X ₀	-183.0 psi
TCUT	None
LTYPE	2.0
K	1.0 (No Lode angle dependence)
ASSOC	0 (Associative)
INITIAL COMPACTION	None

Figure 13. ESR cap model versus ABAQUS cap model (K cycle data)

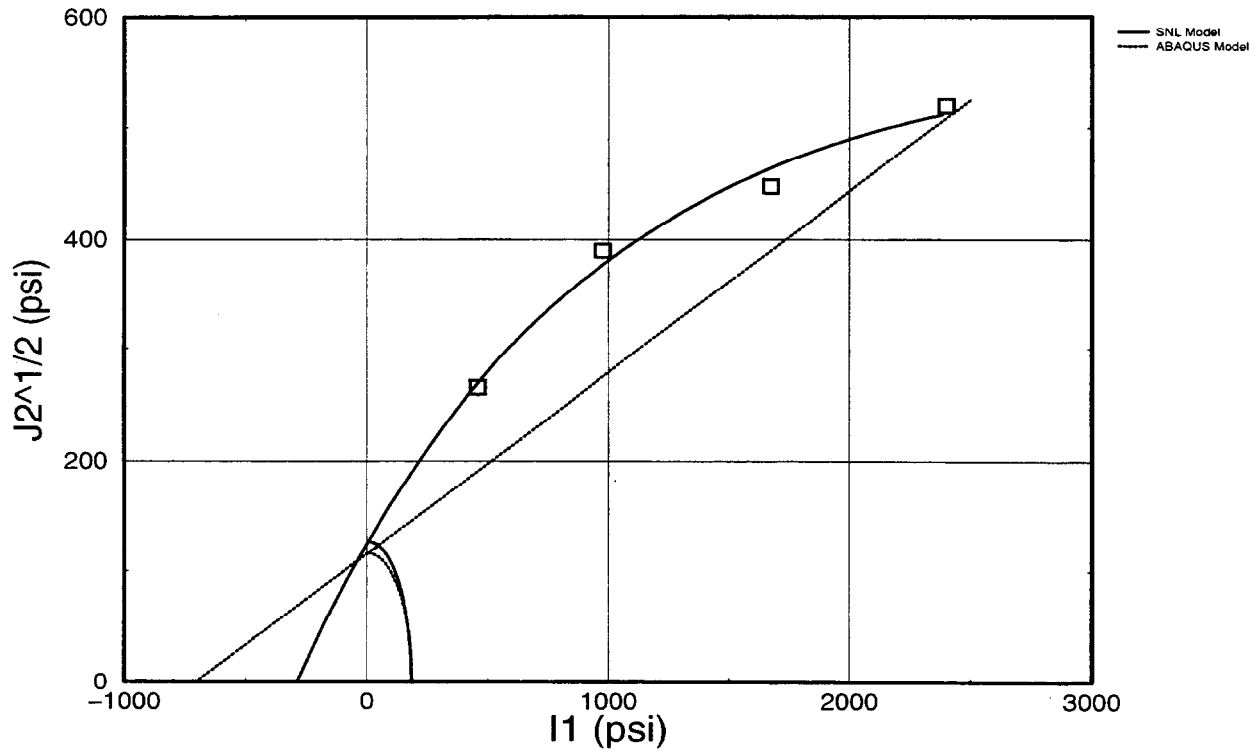


Figure 14. Measured versus predicted uniaxial strain response (K cycle runs)

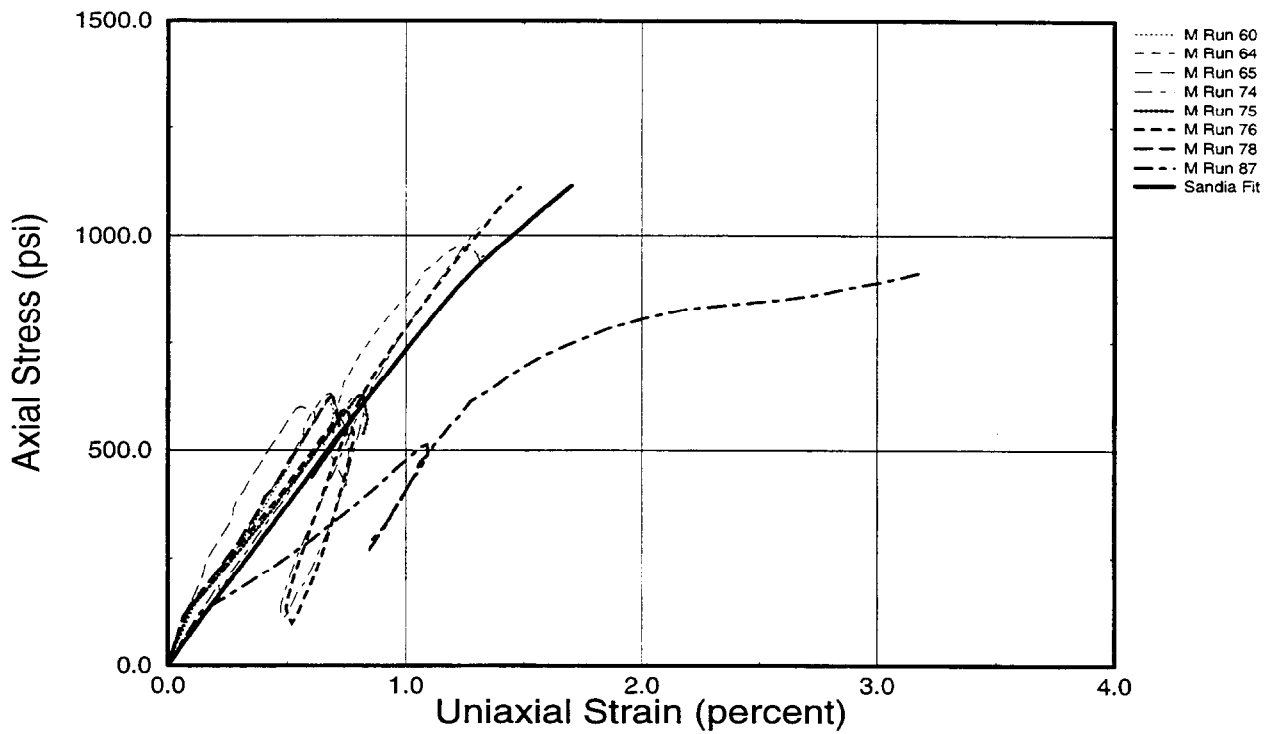


Table 13: Layer L Diatomite Parameter Values for ABAQUS Model

Parameter	Value
Bulk Modulus	56,768 psi
2G	96,068.0 psi
d	247.0 psi
β	50.2 degrees
R	0.23
α	0.01
K	1.0
Hardening	(psi)
0.0	61.0
0.0032	200.0
0.0065	600.0
0.0165	1100.0
0.0205	1400.0

Table 14: Layer L Diatomite Parameter Values for ESR Model

Parameter	Value
Bulk Modulus	56,768.0 psi
2G	96,068.0 psi
A	1235.0 psi
B	3.054-04 1/psi
C	937.51 psi
D ₁	2.8E-05 1/psi
D ₂	0.0 1/psi ²
R	2.5
W	0.08
X ₀	-183.0 psi
TCUT	None
LTYPE	2.0
K	1.0 (No Lode angle dependence)
ASSOC	0 (Associative)
INITIAL COMPACTION	None

Figure 15. ESR cap model versus ABAQUS cap model (L cycle data)

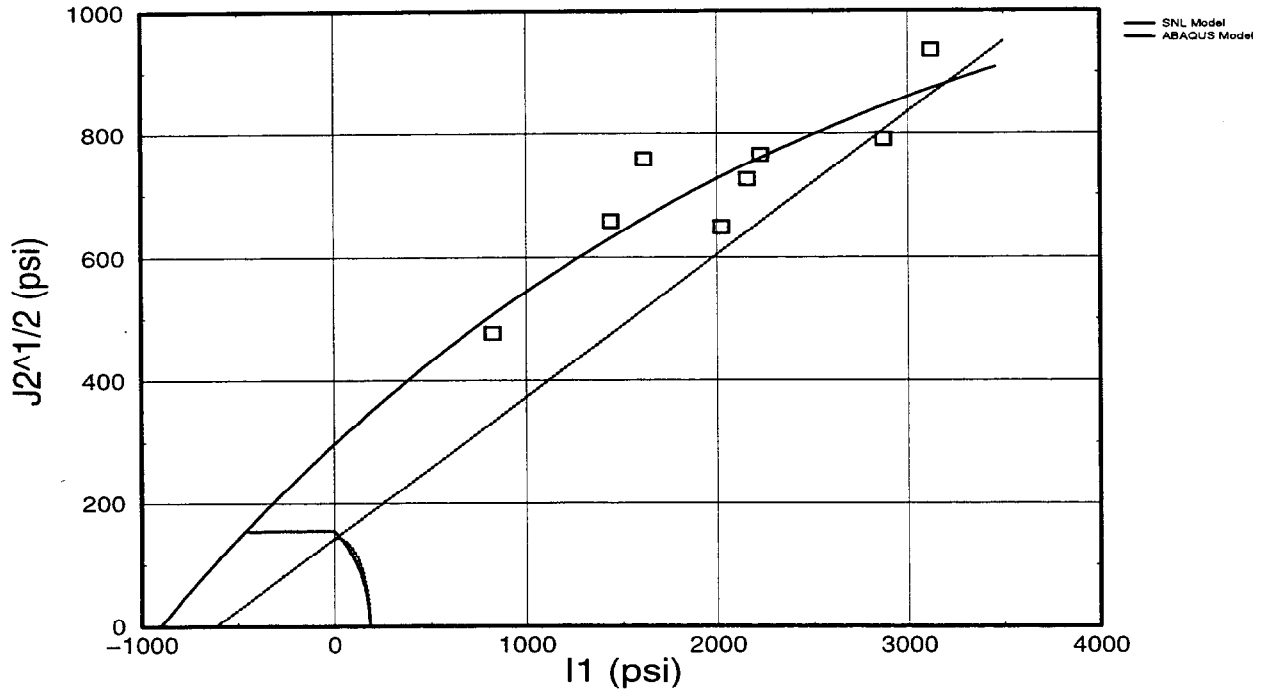
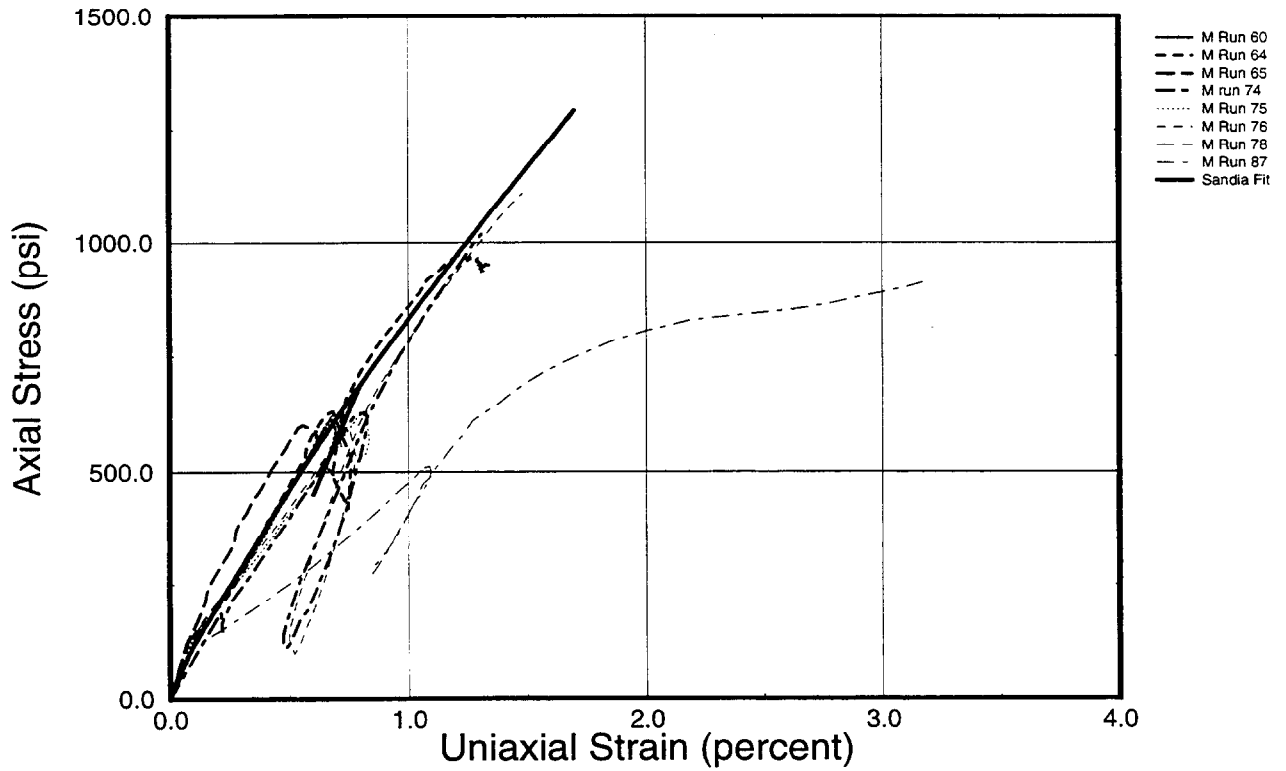


Figure 16. Measured versus predicted uniaxial strain response (L cycle runs)



Conclusion

The geomechanical finite element simulations of reservoir compaction and surface subsidence at the Belridge Diatomite Field (e.g., Hansen et al., 1995; de Rouffignac et al., 1995; Fredrich et al., 1996, 1998) depend fundamentally on: (1) the mechanical loading, which is a direct function of the reservoir pressure history as derived from two- and three-dimensional reservoir simulations; and (2) the material model and constitutive parameters of the reservoir and overburden rock.

Regarding the latter, the following is recommended to improve the accuracy and usefulness of the geomechanical simulations specific to the Belridge Diatomite Field, Section 33:

- The fit to the shear failure surface for several cycles (H, K, L, M) would be better constrained with additional data at low stresses. Fits for all cycles would be improved by the addition of tensile strength data. Duplicate tests should be performed to assess reproducibility.
- Additional conventional triaxial compression tests to failure for cycles H and I are required over the stress range of interest to adequately constrain the shear failure surface. The data available to fit the shear failure surface for cycle K were also limited. Again, duplicate tests should be performed.
- Two uniaxial strain tests should be conducted to large strains (~20-30%) to determine the cap constitutive parameters accurately for cycles H, I, K, and L. Additional tests to larger axial strains are desirable for cycles G and M. The test data, and therefore the derived constitutive parameters, would probably be more robust if these tests were conducted in a triaxial cell with internal instrumentation rather than in an oedometer.
- In the event that additional geomechanical simulation are to be performed on different areas of the field such as Middle Belridge or North Belridge, then scoping tests should be performed to determine the extent to which the existing material models (which are mostly based on core samples obtained from Section 33 in South Belridge) are applicable.
- Finally, it would be useful to perform some minimal parameter sensitivity studies to investigate how sensitive the geomechanical simulations are to the particular constitutive properties describing the various diatomite cycles. For example, the most significant difference between the ESR Cap Model parameters used originally (e.g., Fredrich et al., 1996) and those determined here are that the latter tend to have substantially reduced tensile strengths and, in some cases, elevated failure envelopes at intermediate stresses. This is a direct consequence of the use of a non-linear failure envelope in the ESR Cap Model, which is clearly required to fit the experimental data. (Also, in some cases, the previous fit to the shear failure data (de Rouffignac, 1995) differed significantly from the least squares fit to the data. This resulted from an attempt to constrain the tensile strength to what was perceived as a more realistic value than that indicated by the least squares fit to the data (G.L. Deitrick, personal communication, 1996)). It would be useful to perform an idealized simulation using an idealized pore pressure drawdown and pressure maintenance history to investigate the sensitivity of the results to the two different parameter fits.

References

1. de Rouffignac, E.P., J.M. Kararikas, P.L. Bondor, and S.K. Hara. "Subsidence and well failure in the South Belridge Diatomite Field," SPE 29626, *Proc. 1995 SPE Western Regional Meeting*, Bakersfield, CA, March 8-10, 1995.
2. Fossum, A.F., "Parameter Estimation for an Internal Variable Model Using Nonlinear Optimization and Analytical/Numerical Response Sensitivities," *J. Engr. Mat. Tech.*, 119, 337-345, 1997
3. Fossum, A.F., P.E. Senseny, T.W. Pfeifle, and K.D. Mellegard. "Experimental Determination of Probability Distributions for Parameters of a Salem Limestone Cap Plasticity Model," *Mech. of Mat*, 21, 119-137, 1995
4. Fossum, A.F., "Extended Sandler-Rubin (ESR) Cap Plasticity Model," (in preparation), 1998.
5. Fredrich, J.T., J.G. Arguello, B.J. Thorne, W.R. Wawersik, G.L. Deitrick, E.P. de Rouffignac, L.R. Myer, and M.S. Bruno. "Three-Dimensional Geomechanical Simulation of Reservoir Compaction and Implications for Well Failures in the Belridge Diatomite," SPE 36698, *Proc. 1996 SPE ATCE*, Denver, CO., Oct 6-9, 1996
6. Fredrich, J.T., Deitrick, G.L., Arguello, J.G., and De Rouffignac, E.R., "Reservoir Compaction Surface Subsidence, and Casing Damage: A Geomechanics Approach to Mitigation and Reservoir Management," paper SPE 47284 presented at the SPE/ISRM Eurock '98 conference, Trondheim, Norway, 8-10 July 1998.
7. Hansen, K.S. M. Prats, and C.K. Chan. "Modeling Reservoir Compaction and Surface Subsidence at South Belridge," SPEPF, Aug., 134-143, 1995
8. Myer, L., et al., "Use of Visualization Techniques in Analysis of Well Failures in Diatomite Reservoirs," *The Leading Edge*, p. 185, March 1996.
9. Sandler, I.S. and Rubin, D., "An Algorithm and a Modular Subroutine for the Cap Model," *Int. J. Num. Anal. Meth. Geo.*, 3, p. 173, 1979.

External Distribution:

Aera Energy LLC (5)
5060 California Ave.
P.O. Box 11164
Bakersfield, CA 93389-1164
Tom Moroney (2)
Bob Gwinn
Phil Warren
Tony Murer

Shell E&P Tech. Co. (4)
BTC 1136
P.O. Box 481
Houston, TX 77001
Greg Deitrick (2)
Eric de Rouffignac
Kirk Hansen

Chevron Petroleum Tech. Co. (3)
1300 Beach Blvd.
P.O. Box 446
La Habra, CA 90631
Russ Ewy
Craig Bovberg
Ray Tang

Greg Mazmanian (1)
Chevron USA Prod. Co.
4900 California Ave.
Bakersfield, CA 93309

Chuck Dobie (1)
Crutcher-Tufts Prod. Co.
5500 Ming Ave., Suite 210
Bakerfield, CA 93309

Bob Shore (1)
Bakersfield Energy Resources
2131 Mars Court
Bakersfield, CA 93308

Kalon Degenhardt (1)
Texaco Exploration and Production Inc.
Box 519TX
Bakersfield, CA 93308

Larry Myer (1)
Lawrence Berkeley Laboratory
Earth Sciences Division, MS 50C
Berkeley CA 94720

Mike Bruno (1)
Terralog Technologies
332 E. Foothill Blvd, Suite B
Arcadia CA 91006

U.S. Department of Energy (4)
National Petroleum Technology Office
P.O. Box 3628
Tulsa, OK 74101
Jerry Casteel (2)
Bob Lemmon (2)

David Parrish (1)
CenterLine Consulting
Professional Offices
P.O. Box 330
Rapid City, South Dakota 57709

J. Casey Moore (1)
Earth Sciences
University of California
Santa Cruz, CA 95064

Internal Distribution:

MS0751 L.S. Costin, 6117 (1)
MS0751 J.T. Fredrich, 6117 (5)
MS0751 W.A. Olsson, 6117 (1)
MS0751 D.S. Preece, 6117 (1)
MS0751 D.H. Zeuch, 6117 (1)
MS0751 6117 File (5)
MS0750 D.J. Borns, 6116 (1)
MS0750 J.C. Lorenz, 6116 (1)
MS0701 File, 6100 (1)
MS0443 A.F. Fossum, 9117 (5)
MS0443 J.G. Arguello, 9117 (1)
MS0443 J.F. Holland, 9117 (1)
MS-443 H.S. Morgan, 9117 (1)
MS0443 C.M. Stone, 9117 (1)
MS9018 Central Technical Files, 8940 (2)
MS0899 Technical Library, 4916 (2)

MS0619 Review and Approval Desk, 12690 (2)
for DOE/OSTI